Development of a new car C-pillar made of sandwich structures

Journal of Sandwich Structures & Materials

Valladares et al.

David Valladares[1] Luis Castejon[1] Jesus Cuartero[1] Hugo Malon[1] David R Angulo[1] Stefan Ilijevic[2] Xavier Agustin[2]

[1]. Escuela de Ingeniería y Arquitectura, University of Zaragoza, Zaragoza, Spain
[2]. SEAT, S.A., Barcelona, Spain[AQ1]

Luis Castejon, University of Zaragoza, Maria de Luna s/n, Zaragoza 50018, Spain. Email: luiscast@unizar.es

ABSTRACT

This article presents the experimental–numerical analysis carried out in order to achieve a new automotive component, consisting of a C-pillar constituted by sandwich structure made of steel skins and a rigid foam core. The objective was to achieve a lighter component than the corresponding reference configuration, yet fulfilling mechanical requirements related to stiffness and strength. In fact, the new C-pillar should be at least stiffer and stronger than the reference component. In addition, the final price of the new C-pillar should be in the same range as the price of the initial component, which made it impossible to apply expensive materials such as carbon fiber composite materials.

Keywords: C-pillar , sandwich structure , automotive component , steel skin , epoxy foam

Introduction

The existing weight reduction trend within the automotive sector is a constant challenge that is driving new developments [1]. This is due to the fact that a weight reduction implies a lower consumption of fuel and, therefore, lower polluting emissions. However, there must be a balance between the weight reduction pursuit in a car and the existing requirements in terms of stiffness and strength, mainly in order to resist adequately different types of crashes that a car may encounter [2].

Main car manufacturers are researching on the application of advanced materials and manufacturing processes to the construction of new car components. Examples of new materials substituting the traditional standard steel are carbon fiber composite materials, or alternative metals to steel, such as aluminum or magnesium [3]. However, these materials have a specific price per kilogram that far exceeds that of steel, even by several orders of magnitude, as in the case of carbon fiber composite materials. In this context, sandwich structures are being applied to car panel construction not only due to their acoustic properties [4] but also due to their high stiffness and high flexural and bucking strength characteristics per kilogram weight [5]. Aluminum or composite skins combined with a polyurethane, polyvinyl chloride (PVC), or even aluminum foam core are usual examples of car sandwich panels [6]. In addition, different foam types have been applied to automotive-specific components in order to improve their ability to absorb crash energy [7] and to dampen vibrations [8].

However, unlike what has been collected in the state of the art, this article explains the development of a component that does not have a flat panel shape, but it belongs to a curved C-pillar of a car, which for the first time has been constructed by means of the application of a sandwich structure, made of steel skins and epoxy foam core. By means of this new concept of C-pillar, a significant weight reduction was expected in comparison to the existing C-pillar made of stamped steel. It must be taken into account that C-pillar components have a great influence on the torsional stiffness of the car. Moreover, the new C-pillar will provide greater stiffness and strength than the current component, having a final price in the same order of magnitude, thanks to the application of steel and epoxy resin as constituent materials and standard manufacturing processes. High-priced raw materials have been avoided in this research.

The design criteria applicable to the new C-pillar will be presented, which are related to geometrical limitations and mechanical stiffness and strength. First, a numerical optimization of the new C-pillar was carried out by means of the finite element method (FEM). Second, three prototypes were manufactured, thanks to the construction of low cost molds. Finally, the final verification tests were developed by means of the built prototypes. These tests provided experimental validation of the mechanical behavior of the developed C-pillars and also served to obtain a numerical–experimental correlation between numerical calculations and experimental results.

Objective

This paper is focused on the introduction of innovative sandwich structures in C-pillar's components of a passenger car for the improvement of its static torsional stiffness and strength, also achieving a weight reduction with respect to the original design. The University of Zaragoza (Spain) worked in close collaboration with the Spanish car manufacturer SEAT, and the geometry and characteristics of a SEAT's small family car model (according to European New Car Assessment Programme ~~European Nnnew Ccear Aaassessment Ppprogramme~~ ~~EuroNCAP~~~~EuroNCAP~~ class) were taken as a reference for carrying out this analysis. [AQ2]Obtained results are applicable to other car categories, and future structural developments will benefit from this research, though.

It should be noted that a higher static torsional stiffness of the car will have a positive effect on basic aspects of the vehicle's performance [9,10] such as its handling, stability, durability, noise, and vibrations, among others, which therefore could also be pointed out as the ultimate aim in this research.

Design requirements in C-pillar optimization

The initial composition of C-pillar in the specific vehicle analyzed is shown in Figure 1. Concretely, the set located at the left side of the car has been analyzed and basically consists of two stamped sheet metal parts joined together by means of spot welds. The part at the bottom is assembled to the rear left wheel tower, and the part at the top is supporting the rear roof rail. These two curved U-shaped parts (from now on will be referred to as "upper C-pillar" and "lower C-pillar") are also spot welded by means of their side flanges to the inner left flank of the car body. An additional intermediate part connects the top end of upper C-pillar to the roof rear rail (see part "assembly to roof" in Figure 1). The first design requirement was to maintain the exterior geometry of the original C-pillar as well as the specific positions of the spot-welded joints so as to be able to substitute the current design for a new one, without affecting other components in the global assembly of the body-in-white (BIW) of the car. Therefore, sandwich structures in the new proposed designs were oriented inwards from the outer surfaces in current upper and lower C-pillars (see Figure 2).

Figure 1. CAD model of BIW's sheet steel parts comprising the left C-pillar. Reference points 1 to 6.

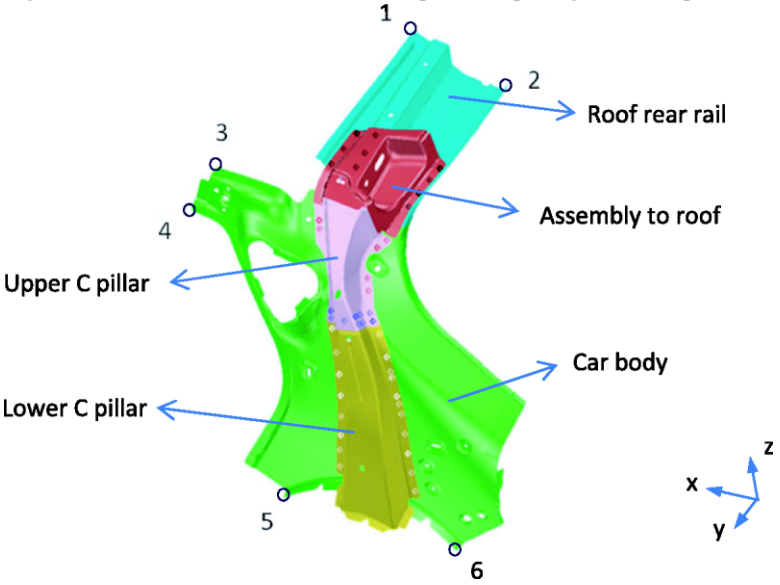

Figure 2. (a) Upper C-pillar, (b) lower C-pillar, and (c) complete C-pillar.

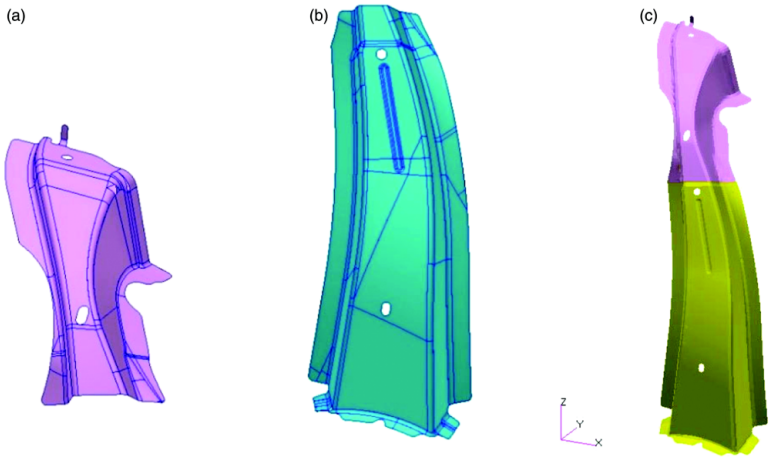

In relation to strength and stiffness constraints, the new C-pillar designs were focused on achieving an improved torsional rigidity. This means that, in relation to the initial design's torsional rigidity results, a higher torsional rigidity (and therefore a better structural performance) should be reached in the new designs. Car manufacturers normally assess the structural performance of their vehicles by means of test procedures practiced on the complete BIW, which include static torsion and static bending tests and modal analysis tests [9,10]. In the case of torsional rigidity tests, a test bench supports the BIW, and a torsion load is applied at the front or at the rear of the vehicle, and then, the torsional angle reached is measured.

In this research, two approaches were considered for assessing the torsional rigidity at C-pillars. In the first approach, the manufacturer supplied the displacement results obtained with the initial design at several reference points when a torsional load is applied to the vehicle. These displacement values were imposed as boundary conditions on the numerical models created, which made possible to assess the structural response in upper and lower C-pillars. Table 1 shows the displacement values obtained from the torsional test of the vehicle at six reference points (see Figure 1). Reference points 1 and 2 were taken from the middle longitudinal section at the roof rear rail, and reference points 3, 4, 5, and 6 were taken from the car body. In the second approach, a torsional angle of 1° was directly imposed on the top of upper C-pillar, and then, the structural response was numerically measured in the components.

Table 1. Displacement values at reference points 1 to 6 obtained from the torsional test of the vehicle.

Reference point	X displacement (mm)	Y displacement (mm)	Z displacement (mm)
1	0.0157	–9.9139	0.0873
2	0.0618	–9.8305	0.2269
3	0.1895	–9.7929	–1.0059
4	–0.0493	–9.2162	–1.5271
5	–0.4488	–4.0359	–2.5786
6	–0.5446	–4.1025	–2.6944

Concerning weight reduction, the new design proposals were focused on using as less material as possible maintaining the same or a higher torsional rigidity. The use of sandwich structures consisting of two outer stamped steel sheets and a polymeric material core allowed to reduce the gauge of the steel sheets at a feasible minimum, while the second moment of area in the pillar components is increased [11]. The manufacturer required a minimum thickness value of 0.4 mm for each sandwich's steel sheet due to manufacturability limitations present in resistance spot welding. Moreover, the steel grades used in the initial design of C-pillars were kept for the new designs.[AQ3]

The new design was intended to be added to the car structure without major changes in the existing manufacturing process. As a consequence, the spot welding positions were maintained in their original coordinates for all the numerical models.

Methodology for analysis and optimization of C-pillar by the FEM

Design and evaluation approaches for the new C-pillars

In the first place, and parting from the original geometry, three different possibilities were considered for modeling the C-pillar components as FE submodels. It was taken into account that upper and lower C-pillars are part of the BIW that constitutes the structure of the vehicle and are therefore working as structural elements in combination with adjacent components. In this sense, not only should C-pillar's components perform correctly as individual parts but also should work adequately combined and once fixed to the car structure. The following analysis strategies were then considered:

1. Structural analysis assessing upper and lower C-pillars working independently.
2. Structural analysis assessing upper and lower C-pillars working combined but not connected to the vehicle structure.
3. Structural analysis assessing upper and lower C-pillars working together and welded to the adjacent structural parts at the top and at the bottom of the vehicle (assembly to roof part and to rear wheel cover part, respectively).

Table 2 below collects the design approaches that were considered in the numerical models and the analyses carried out for each design.

Table 2. New C-pillar designs analyzed and numerical models' configuration.

Design approach/numerical model	a) Pillars analyzed independently	b) Pillars analyzed together	c) Pillars analyzed together with adjacent parts
1. Original geometry changing initial thicknesses in steel sheets	X	X	
2. Sandwich structures with 3-mm polymer sandwich core	X	X	
3. Sandwich structures with 10-mm rigid polymer foam sandwich core	X	X	
4. Design no. 2 with cross-shaped stamping carried out on inner skins	X	X	
5. Design no. 3 with cross-shaped stamping carried out on inner skins	X	X	
6. Mixed C-pillar: no. 3 sandwich lower pillar with stamped steel upper pillar		X	
7. Design no. 3 with new connection region between upper and lower pillars, with flanges at both inner and outer skins		X	X

Design approach no. 1 was the simplest one and consisted in checking the performance of the initial design using different steel sheet's thicknesses. Designs no. 2 and 3 were the two possibilities of sandwich structure analyzed, considering a different core material and thickness at each case. Designs no. 4 and 5 included cross-shaped stamped geometries in the inner steel sheets of the sandwich configurations and was intended to assess their work hardening effect over the torsional rigidity of the components. In this case, the outer sheet geometries were maintained as original. Design no. 6 studied the combination of one upper or lower original C-pillar with another upper or lower no. 3 sandwich C-pillar. Design no. 7 included new geometries for the assembly region between upper and lower C-pillars, intended to correct the low rigidity sections in the spot-welded area and achieving a better integration of the sandwich structures for performing as a whole. It also included welding flanges in both the inner and outer sheet of the sandwich in order to strengthen the assembly to adjacent components.

FE mesh models developed

In a first step, the original computer-aided design (CAD) models of the components were supplied by the manufacturer, which included the welding points' positions for joining them. [AQ4]The FE numerical models were then created using a commercial pre-processor software and finally analyzed with commercial FE codes. Since the main objective was to assess the torsional rigidity of the components in normal driving conditions, which was far from plasticity or material failure in the original design, the numerical simulations were performed as linear static stress analyses. In models no. 1, 2, and 3, the steel stamped sheets were modeled using three-dimensional first-order interpolation shell elements, which were mainly four-node shell elements and three-node ones for highly curved surfaces and mesh transition regions. These elements were used with reduced integration, and their thicknesses were defined through the section property definition of the code. The six displacement and rotational degrees of freedom were available for these shell elements, and transverse shear deformation was also computed in them. The sandwich cores filling the components in models 2 and 3 were modeled with first-order interpolation solid continuum elements, mainly by means of eight-node linear brick elements with reduced integration and six-node linear triangular prism elements in mesh transition regions. Since their geometry represents the volume of the material, these solid elements did not require thickness definition. Consequently, they only had three displacement degrees of freedom available in the analysis. Welded joints were modeled using rigid multi-point constraints between two nodes in different parts.

Two different designs were considered for the sandwich structures:

1. 3-mm-thick core made of polymer (design approaches no. 2 and 4, see Figures 3 and 5) and
2. 10-mm-thick core made of rigid polymer foam (design approaches no. 3 and 5, see Figures 4 and 6).

An isotropic linear elastic material model was considered for the steel sheets and the polymers' characterization. This numerical model was appropriate because it is normally valid for small elastic strains of less than 5%, and the considered load cases simulated the torsional performance of the vehicle in load situations not intended to reach permanent strains. Table 3 shows the mechanical properties of the materials considered in the numerical models. The values considered for PVC or polyester polymer and rigid polymer were normal medium values that can be reached with these material types.

Table 3. Mechanical properties of materials considered in the numerical models.

Component	Material	Density (kg/m^3)	Elastic modulus (MPa)	Poisson's ratio	R_e (MPa)	R_m (MPa)	A_{80} (%)
Lower C-pillar	Steel HC 260 LA/1.0480 (EN 10268)[12]	7800	210,000	0.3	260–330	350–430	26
Upper C-pillar	Steel HC 260 LA/1.0480 (EN 10268)	7800	210,000	0.3	260–330	350–430	26
Assembly to roof	Steel DX 53D/1.0951 (EN 10346)[13]	7800	210,000	0.3	140–260	270–380	30
Rear wheel cover	Steel HC 220 B/1.0396 (EN 10268)	7800	210,000	0.3	220–270	320–400	32
Sandwich core designs no. 2 and 4	Polymer: PVC or polyester	1500	2800	0.3	–	–	–
Sandwich core designs no. 3, 5, 6 and 7	Rigid polymer foam	130	200	0.3	–	–	–

PVC: polyvinyl chloride.

The complex geometries present in design approaches no. 4 and 5 and the cross-shaped notches stamped at the inner sheets of the sandwich made necessary a major use of 3-node shell elements (first-order interpolation with reduced integration) for modeling the skins and 10-node quadratic solid tetrahedrons (solid continuum elements with

second-order interpolation) for the cores in order to accurately reproduce the stamped shapes by the mesh models. Similarly, as before, while shell elements required thickness definition, in the case of solid elements, the volume was geometrically meshed, and it was not necessary. As shown in Figure 7, these notches were modeled with a different size depending on the sandwich core thickness. [AQ5][AQ6]All sandwich mesh models used equivalent nodes for bonding the skins to the core. Mesh size ranged approximately from 1.5 to 4 mm in all cases.

Figure 3. Design no. 2's FE models, sandwich structures with 3-mm thermoplastic core. Left: lower C-pillar (outer skin, core, and inner skin) and right: upper C-pillar (outer skin, core, and inner skin).

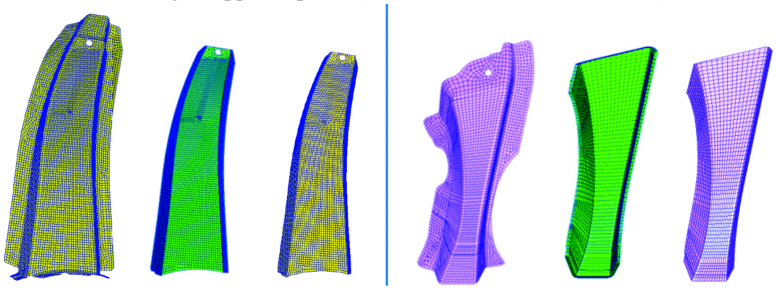

Figure 4. Design no. 3's FE models, sandwich structures with 10-mm polymer foam core. Left: lower C-pillar (outer skin, core, and inner skin) and right: upper C-pillar (outer skin, core, and inner skin).

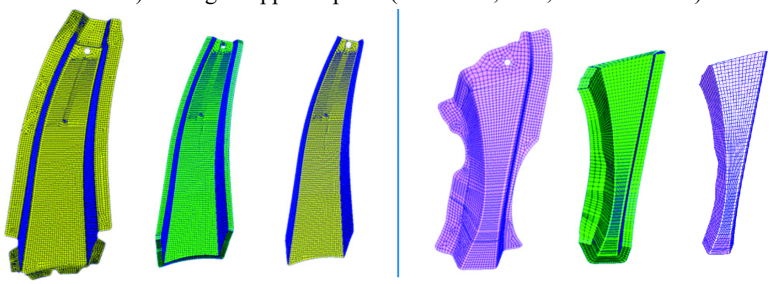

Figure 5. Design no. 4's FE models, sandwich structures with 3-mm thermoplastic foam core. Left: lower C-pillar (outer skin, core, and inner skin) and right: upper C-pillar (outer skin, core, and inner skin).

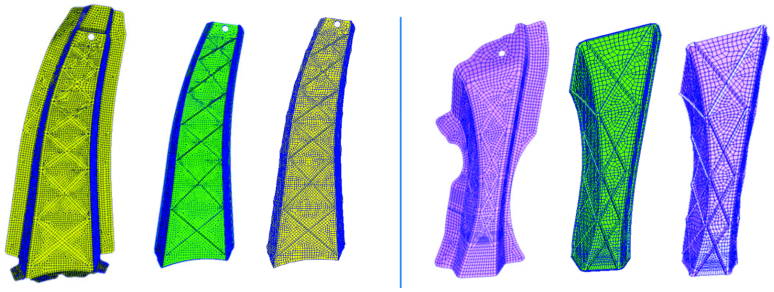

Figure 6. Design no. 5's FE models, 10-mm foam core sandwich with cross-shaped stamping carried out on inner skins. Left: lower C-pillar (outer skin, core, and inner skin) and right: upper C-pillar (outer skin, core, and inner skin).

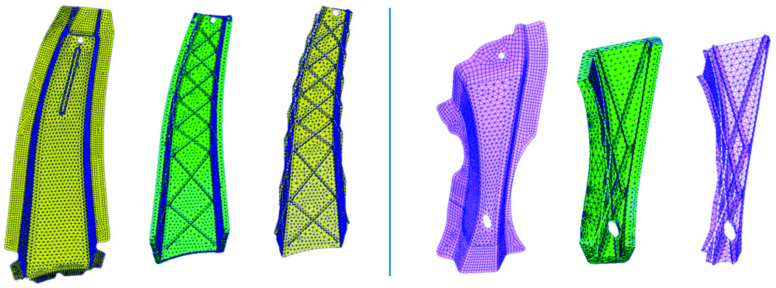

Figure 7. Cross-sectional dimensions of cross-shaped notches located at the inner skins of sandwich pillar designs no. 4 and 5.

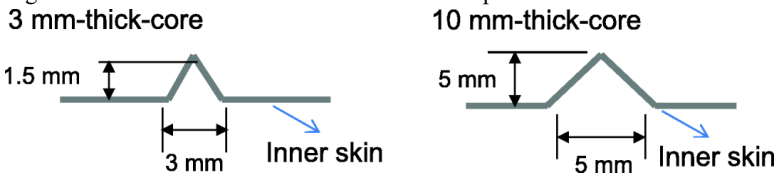

Upper and lower C-pillars were analyzed both working independently and together in design approaches no. 1, 2, 3, 4, and 5. In terms of rigidity, approach no. 3 was considered the optimum one from this series of simulations, and it was therefore used as a basis for the following designs. So, design approaches no. 6 and 7 were only analyzed working together because in these cases it was only necessary to check the combined upper-lower C-pillar behavior. Concerning option no. 6, it combined different pillars from the previous simulations, and as for option no. 7, it introduced several improvements at the transition region between the sandwich pillars and at the pillars' flanges used for welding the pillars to adjacent components.

The torsional rigidity performance of C-pillar was assessed by means of these FE numerical models. In order to validate the numerical results, in the next step, a prototype series based on the optimum C-pillar design was manufactured and later on tested at Zaragoza University's facilities. New steel molds were specifically manufactured for shaping the four steel sheets; then, the core material could be injected between the inner and outer skins before reaching the solid state. The test conditions were numerically simulated, and a high correlation was found between the numerical and the experimental results.

Phase 1: preliminary load cases analyzed and results

Torsional displacements from the complete vehicle tests

In this case, displacement conditions were taken from Table 1, calculating the average relative displacements in x, y, and z direction between reference points 1 and 2 and reference points 5 and 6 (see Figure 1). In a first step, displacements at points 1 and 2 were averaged, and then, the same was performed at bottom points 5 and 6. In a second step, these averaged displacements were used for obtaining the relative displacement between the top and the bottom. The relative displacements were $\Delta x = +0.53$ mm, $\Delta y = -5.8$ mm, and $\Delta z = +2.79$ mm and were used as boundary conditions for the static analyses.

In the independent analysis of upper C-pillar, the displacement field was applied to all the nodes located at the top rim of the component, while the welding points located at the connection with lower C-pillar were constrained in x, y, and z directions. In a similar manner, for the independent analysis of lower C-pillar, the displacement field was applied to the welding points located at the connection with upper C-pillar, while all the nodes at the component's bottom flanges were constrained in x, y, and z directions.

Finally, the analysis of the complete C-pillar was performed applying the displacement field at the upper C-pillar's top rim nodes while constraining the nodes at lower C-pillar bottom flanges. The pillars were connected by means of rigid constraints located at the welding points' nodal positions. Figure 10 shows the boundary conditions for these three situations.

Figure 8. Mesh model for the transition region included at sandwich C-pillar design no. 7. Top: 10-mm core meshes for upper and lower C-pillars and bottom: lower and upper C-pillars with new transition region.

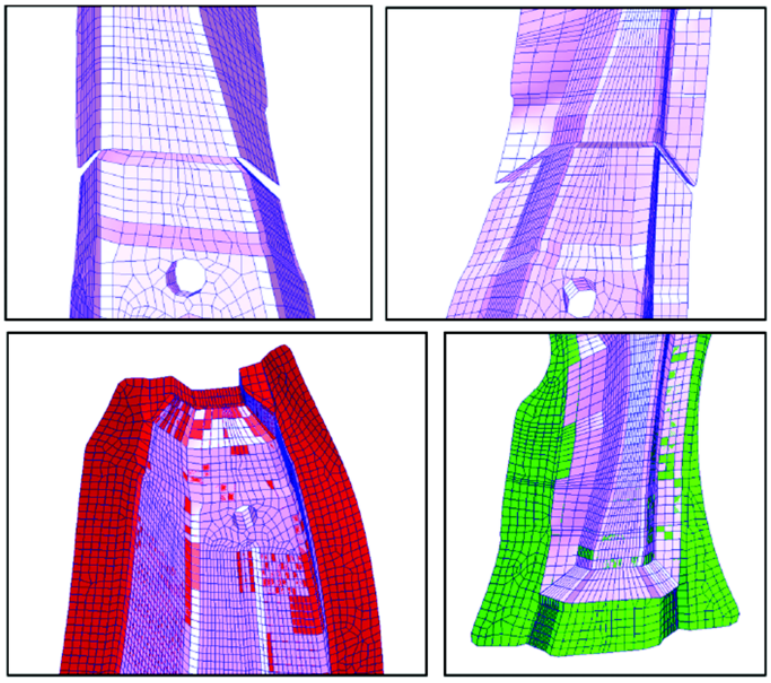

Figure 9. Mesh models for outer and inner skins at sandwich C-pillar design no. 7. Left: upper C-pillar's skins and bottom: lower C-pillar's skins.

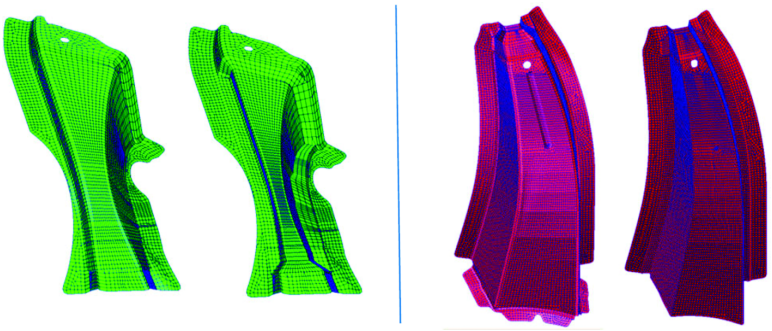

Figure 10. Torsional displacement load cases considered (mm). Left: upper C-pillar, center: lower C-pillar, and right: upper and lower C-pillars connected by welding points.

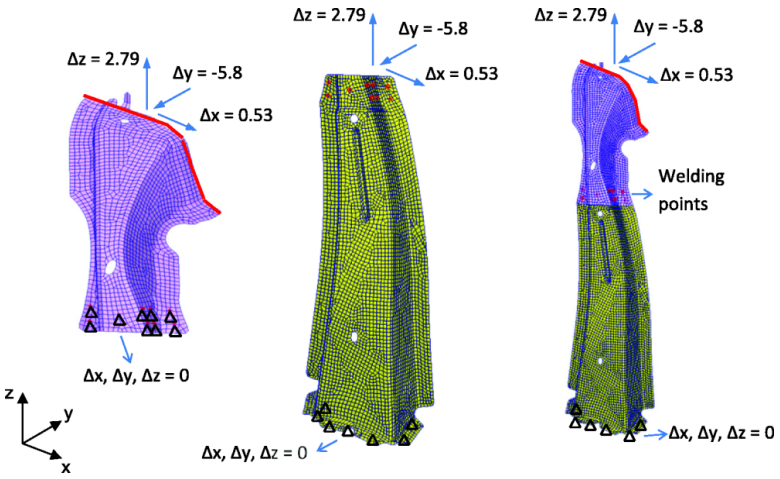

Results from the complete pillar simulation are collected in Table 4. Tables 5 and 6 collect the separated analyses carried out for upper and lower C-pillar, respectively. In all cases, the displacement magnitude considered for calculating the specific stiffness was 6.46 mm.

Table 4. Results for upper and lower C-pillar analyzed connected—torsional displacements load case.

Design	Thickness (mm)				Reaction force (N)	Mass (kg)	Specific stiffness (N/mm·kg)
	Upper C-pillar		Lower C-pillar				
	Outer skin	Inner skin	Outer skin	Inner skin			
Original	1.75		0.8		3928	1.284	473
1a. Original with thickness change	1.85		0.8		4007	1.318	470
1b. Original with thickness change	1.75		0.9		4430	1.370	500
2. Sandwich 3 mm (thermoplastic core)	0.55	0.55	0.4	0.4	4540	1.464	480
3. Sandwich 10 mm (polymer foam core)	0.4	0.4	0.4	0.4	5144	1.041	765
4a. Sandwich 3 mm with cross stamping	0.55	0.55	0.4	0.4	4037	1.472	425
4b. Sandwich 3 mm with cross stamping	0.75	0.75	0.4	0.4	4833	1.600	467
4b. Sandwich 3 mm with cross stamping	0.55	0.55	0.5	0.5	5587	1.631	530
5a. Sandwich 10 mm with cross stamping	0.4	0.4	0.4	0.4	4125.27	1.097	582
5b. Sandwich 10 mm with cross stamping	0.5	0.5	0.4	0.4	5433.43	1.108	759
5c. Sandwich 10 mm with cross stamping	0.4	0.4	0.5	0.5	6199.91	1.205	796

Table 5. Results for upper C-pillar designs analyzed separately—torsional displacements load case.

Design	Thickness (mm)		Reaction force (N)	Mass (kg)	Specific stiffness (N/mm·kg)
	Upper C-pillar				
	Outer skin	Inner skin			
Original	1.75		113,587	0.597	29.44E+3
1a. Original with thickness change	1.85		123,592	0.631	30.30E+3
2a. Sandwich 3 mm (thermoplastic core)	0.55	0.55	55,586	0.467	18.42E+3
2b. Sandwich 3 mm (thermoplastic core)	0.75	0.75	85,732	0.603	22.01E+3
3a. Sandwich 10 mm (polymer foam core)	0.4	0.4	37,213	0.291	19.78E+3
3b. Sandwich 10 mm (polymer foam core)	0.5	0.5	49,436	0.358	21.37E+3

Table 6. Results for lower C-pillar designs analyzed separately—torsional displacements load case.

Design	Thickness (mm)		Reaction force (N)	Mass (kg)	Specific stiffness (N/mm·kg)
	Lower C-pillar				
	Outer skin	Inner skin			
Original	0.8		24,981	0.687	5.63E+3
1a. Original with thickness change	0.9		29,700	0.773	5.94E+3
2a. Sandwich 3 mm (thermoplastic core)	0.4	0.4	35,938	0.997	5.58E+3
2b. Sandwich 3 mm (thermoplastic core)	0.5	0.5	45,832	1.164	6.09E+3
3a. Sandwich 10 mm (polymer foam core)	0.4	0.4	38,082	0.749	7.86E+3
3b. Sandwich 10 mm (polymer foam core)	0.5	0.5	48,172	0.914	8.16E+3

Torsional rotation of 1°

Differently, in this load case, a torsional rotation of 1° was directly imposed to the nodes on the top rim of upper C-pillar and on the top welding points of lower C-pillar in order to assess numerically the torsional response. For upper C-pillar, the rotation was imposed around an axis parallel to "*xy*" plane and at 30° with respect to global "*y*" direction. The rotational axis orientation was chosen for alignment with C-pillar's geometry, after checking from an "*xy*" view that the original upper C-pillar design formed approximately 30° with the global "*y*" axis. Equivalently, for lower C-pillar, the rotation was imposed around an axis parallel to "*xz*" plane and at 30° with respect to the global "*z*" axis. The original lower C-pillar formed approximately 30° with the global "*z*" axis. This latter approach was also used for the complete upper-lower pillar simulation.

The reaction forces were then measured at the constrained nodes located at the bottom (welding point nodes for upper C-pillar and nodes at the bottom flanges for lower C-pillar), whose values allowed to compare the strength and rigidity levels against torsion that are available with different designs. The simulation of a pure rotational deformation in these components is not as realistic a working performance as the previous displacement conditions case, because, as stated before, it is the combined behavior of the BIW's components interacting in the vehicle's structure that gives the actual torsional performance. This simulation approach provided basic information and contributed a new point of view to the design process though. Figure 11 shows the boundary conditions applied to the independently analyzed

pillar's components. Tables 7 and 8 collect the separated analyses carried out for upper and lower C-pillar, respectively.

Figure 11. One-degree torsional rotation load cases. Left: upper C-pillar and right: lower C-pillar.

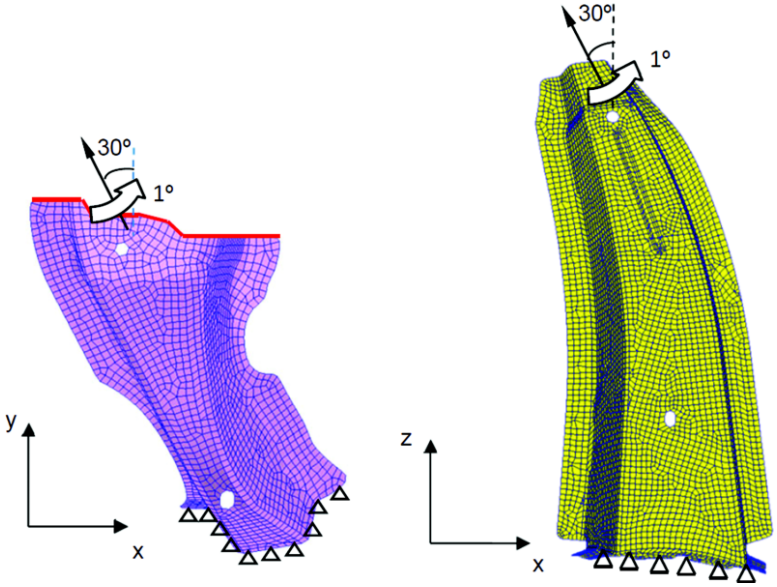

Table 7. Results for upper C-pillar designs analyzed separately—one-degree torsional rotation load case.

Design	Thickness (mm)		Reaction moment (N·mm)	Mass (kg)	Specific stiffness (N·mm/°·kg)
	Upper C-pillar				
	Outer skin	Inner skin			
Original	1.75		64,744	0.597	108.4E+3
1a. Original with thickness change	1.85		69,543	0.631	110.1E+3
2a. Sandwich 3 mm (thermoplastic core)	0.55	0.55	52,289	0.467	111.9E+3
2b. Sandwich 3 mm (thermoplastic core)	0.75	0.75	73,027	0.603	121.1E+3
3a. Sandwich 10 mm (polymer foam core)	0.4	0.4	74,152	0.291	254.6E+3
3b. Sandwich 10 mm (polymer foam core)	0.5	0.5	92,823	0.358	259.2E+3
4a. Sandwich 3 mm with cross stamping	0.55	0.55	45,177	0.470	96E+3
4b. Sandwich 3 mm with cross stamping	0.75	0.75	64,078	0.610	105E+3
5a. Sandwich 10 mm with cross stamping	0.4	0.4	46,663	0.302	154.4E+3
5b. Sandwich 10 mm with cross stamping	0.5	0.5	60,330	0.372	162E+3

Table 8. Results for lower C-pillar designs analyzed separately—one-degree torsional rotation load case.

Design	Thickness (mm)		Reaction moment (N·mm)	Mass (kg)	Specific stiffness (N·mm/°·kg)
	Lower C-pillar				
	Outer skin	Inner skin			
Original	0.8		70,483	0.687	102.5E+3
1a. Original with thickness change	0.9		82,987	0.773	107.3E+3
2a. Sandwich 3 mm (thermoplastic core)	0.4	0.4	99,933	0.997	100.2E+3
2b. Sandwich 3 mm (thermoplastic core)	0.5	0.5	125,581	1.164	107.8E+3
3a. Sandwich 10 mm (polymer foam core)	0.4	0.4	133,731	0.749	178.3E+3
3b. Sandwich 10 mm (polymer foam core)	0.5	0.5	168,416	0.914	184.2E+3
4a. Sandwich 3 mm with cross stamping	0.4	0.4	89,136	1.002	89E+3
4b. Sandwich 3 mm with cross stamping	0.5	0.5	96,932	1.171	96.9E+3
5a. Sandwich 10 mm with cross stamping	0.4	0.4	101,728	0.795	128E+3
5b. Sandwich 10 mm with cross stamping	0.5	0.5	128,741	0.972	132.4E+3

Phase 1 results' assessment

Comparing the different values obtained for the different models in reaction force and moment, mass, and specific stiffness from Tables 4 to 8, it was concluded that design approach no. 3 had the best torsional performance. From Table 4, it can be observed that this 10-mm rigid polymer core sandwich with a 0.4 mm thickness in inner and outer sheets achieved a mass reduction of 0.243 kg (18.9%), a reaction force increase of 1216.22 N (30.9%), and a stiffness increase of 292 N/mm·kg (38.1%) in the connected pillars simulation. Design approach no. 3 required an increase in sheets' thickness (it worked more effectively in lower C-pillar) for achieving as high a force reaction as design no. 2, which penalized its mass and consequently its specific stiffness. The inclusion of cross-shaped stamping at inner skins of sandwich structures no. 4 and no. 5 did not contribute positively neither for the 3-mm thermoplastic core nor for the 10-mm polymer core (observed comparing 4a with 2a, 4b with 2b, 5a with 3a, and 5b with 3b in the tables). Therefore, design options no. 2, 4, and 5 were rejected.

Another interesting result was that the reaction force and specific stiffness in the displacement load case for upper C-pillar provided lower values in the sandwich designs than the original upper C-pillar (see Table 4). Differently, the reaction moment and the specific rotational stiffness reached higher values in all sandwich designs for the torsional rotation load case.

Moreover, the sensitivity to an increase of 0.1 mm in thickness was different in the original upper and lower C-pillars, being the thickness increase for lower pillar which produced the higher stiffness increase in all the simulations. For instance, the specific torsional stiffness increased 1.56% for upper C-pillar and 4.68% for lower C-pillar when a one-degree rotation was applied to each component (0.1 mm thicker).

All in all, and from the basis of design no. 3, the following steps were considered in a second phase of this research:

- To combine the original upper C-pillar with equal and reduced thickness with a sandwich structure for the lower C-pillar.
- To introduce a new geometry in the joint region connecting upper and lower sandwich pillars in order to improve its area moment of inertia. The original region performed as a weak point to flexural loads once sandwich structures were included.

- To include welding flanges for both inner and outer sandwich's skins in order to avoid non-desirable hinge effects.

Phase 2: modified models analyzed and results

Mixed C-pillar: original upper pillar with 10-mm sandwich lower pillar

Here, three different thicknesses (1.75, 1.5, and 1.25 mm) were selected for the original upper C-pillar, while design no. 3 was used for lower C-pillar (10-mm sandwich structure with rigid polymer foam and 0.4-mm-thick steel sheets). Tables 9 and 10 show the results for the mixed C-pillar analyzed complete with welding points in the connection region.

Table 9. Results for mixed C-pillar analyzed connected—torsional displacements load case.

Design	Thickness (mm)			Reaction force (N)	Mass (kg)	Specific stiffness (N/mm·kg)
	Upper C-pillar	Lower C-pillar				
		Outer skin	Inner skin			
6a. Mixed C-pillar	1.75	0.4	0.4	5581	1.347	641
6b. Mixed C-pillar	1.50	0.4	0.4	5334	1.262	654
6c. Mixed C-pillar	1.25	0.4	0.4	5048	1.176	664

Table 10. Results for mixed C-pillar analyzed connected—one-degree torsional rotation load case.

Design	Thickness (mm)			Reaction moment (N·mm)	Mass (kg)	Specific torsional stiffness (N/°·kg)
	Upper C-pillar	Lower C-pillar				
		Outer skin	Inner skin			
6a. Mixed C-pillar	1.75	0.4	0.4	16,382	1.347	12,162
6b. Mixed C-pillar	1.50	0.4	0.4	12,995	1.262	10,297
6c. Mixed C-pillar	1.25	0.4	0.4	9954	1.176	8464

Sandwich pillars with modified connection region

The modifications included in design approach no. 7 are shown in Figure 8 and Figure 9. In this case, the sandwich structure was extended to the connection region between upper and lower pillars. Tables 11 and 12 show the results obtained with this configuration and also the stiffness improvement obtained by changing upper or lower sheets' thicknesses from 0.4 to 0.5 mm.

Table 11. Results 10-mm core sandwich, modified connected region—torsional displacements load case.

Design	Thickness (mm)				Reaction force (N)	Mass (kg)	Specific stiffness (N/mm·kg)
	Upper C-pillar		Lower C-pillar				
	Outer skin	Inner skin	Outer skin	Inner skin			
7a. Sandwich 10 mm (rigid foam core)	0.4	0.4	0.4	0.4	6340	1.040	952
7b. Sandwich 10 mm (rigid foam core)	0.5	0.5	0.4	0.4	6774	1.106	947
7c. Sandwich 10 mm (rigid foam core)	0.4	0.4	0.5	0.5	7518	1.204	966

Table 12. Results 10-mm core sandwich, modified connected region—one-degree torsional rotation load case.

Design	Thickness (mm)				Reaction moment (N·mm)	Mass (kg)	Specific stiffness (N/°·kg)
	Upper C-pillar		Lower C-pillar				
	Outer skin	Inner skin	Outer skin	Inner skin			
7a. Sandwich 10 mm (rigid foam core)	0.4	0.4	0.4	0.4	40,023	1.040	38,484
7b. Sandwich 10 mm (rigid foam core)	0.5	0.5	0.4	0.4	47,302	1.106	42,738
7c. Sandwich 10 mm (rigid foam core)	0.4	0.4	0.5	0.5	41,886	1.204	34,786

Finally, and in order to check the torsional response at a higher structural level, this same C-pillar configuration was analyzed including components adjacent to upper and lower C-pillar and including welding flanges for both the inner and outer skins of the sandwich (which added a little more mass). Figure 12 shows the new FE model with the load cases considered, and Tables 13 and 14 collect the results. In the torsional displacements case, the displacements considered were the same as in previous models: $\Delta x = 0.5$ mm, $\Delta y = -5.8$ mm, and $\Delta z = 2.79$ mm, and they were applied to the nodes at the rim of the "assembly to roof" component. In the torsional rotation case, the 1° rotation was directly applied to these rim nodes and around y axis. The constrained nodes were also considered differently, constraining x, y, and z displacements in the contour of the "rear wheel cover" component shown in Figure 12.

Figure 12. Left: torsional displacements (mm) and right: torsional angle.

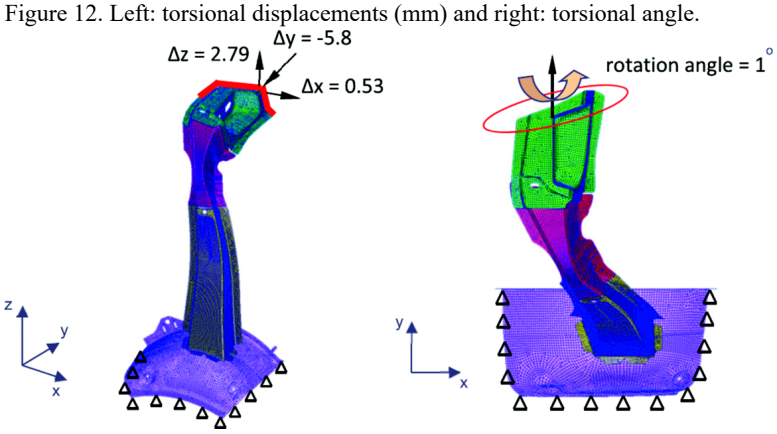

Table 13. Results for FE models with adjacent components—torsional displacements load case.

Design	Thickness (mm)				Reaction force (N)	Mass (kg)	Specific stiffness (N/mm·kg)
	Upper C-pillar		Lower C-pillar				
	Outer skin	Inner skin	Outer skin	Inner skin			
Original C-pillar	1.65		0.8		140.6	1.254	17.3
7a. Sandwich 10 mm (rigid foam core)	0.4	0.4	0.4	0.4	195.2	1.062	28.4

Table 14. Results for FE models with adjacent components—one-degree torsional rotation load case.

Design	Thickness (mm)				Reaction moment (N·mm)	Mass (kg)	Specific torsional stiffness (N/°·kg)
	Upper C-pillar		Lower C-pillar				
	Outer skin	Inner skin	Outer skin	Inner skin			
Original C-pillar	1.65		0.8		2642	1.254	2106.4
7a. Sandwich 10 mm (rigid foam core)	0.4	0.4	0.4	0.4	10,362	1.062	9756.1

Phase 2 results' assessment

Concerning no. 6 mixed configuration, while in the torsional displacement load case the reaction force was higher (only for gauges 1.75 mm and 1.5 mm in upper pillar), in all the simulations, the resulting specific stiffness was lower than the values previously obtained with a complete sandwich configuration. Moreover, in the torsional rotation load case, not only the reaction moment values but also the specific stiffness ones were lower than the complete sandwich configuration. Therefore, this possibility was finally rejected.

On the contrary, the improvement in the connection region of configuration no. 7 gave quite better specific stiffness results, increasing 24% in the displacement load case and 35% in the torsional rotation load case. The 0.1 mm sheet gauge increase worked better applied to the lower pillar in the displacement load case and applied to the upper pillar in the torsional rotation load case.

It was concluded that sandwich structures with 0.4-mm-thick steel sheets and 10-mm rigid foam core, including the new connection region and welding flanges for both inner and outer skins, were the best design option: not only did they have the lowest mass values, but they also achieved quite higher reaction forces and moments. This performance was checked in a more complete structural model including two adjacent parts, obtaining a 64% increase in specific stiffness for the vehicular displacements load case and a 363% increase in specific torsional stiffness for the rotational angle load case. The main features of the new design are shown and compared with the original C-pillar in Table 15.

Table 15. Main features of the new design compared with the original design for C-pillar.

Design	Upper C-pillar	Lower C-pillar	Mass (kg)	Specific stiffness (N/mm·kg)	Specific torsional stiffness (N/°·kg)
Original C-pillar	Steel HC 260 LAThickness = 1.65 mm	Steel HC 260 LAThickness = 0.8 mm	1.254	17.3	2106.4
New C-pillar (sandwich design 7a)	*Sandwich skins:* –Steel HC 260 LA–Thickness = 0.4 mm–Improved upper–lower joint region–Welding flanges for inner and outer skins*Sandwich core:* –Rigid polymer foam–Thickness = 10 mm	*Sandwich skins:* –Steel HC 260 LA–Thickness = 0.4 mm–Improved upper-lower joint region–Welding flanges for inner and outer skins*Sandwich core:* Rigid polymer foamThickness = 10 mm	1.062	28.4	9756.1

Experimental validation of the FE sandwich model with prototype tests

A sandwich C-pillar prototype was manufactured and later on tested, in order to validate the stiffness response obtained in previously analyzed FE models, by means of an adequate experimental–numerical correlation. The prototype was intended to represent the numerical model shown in Figure 12. Preliminarily, it was necessary to manufacture four die-punch pairs required for the stamping process of all inner and outer steel sheets. CAD models of the sandwich's skins developed in design no. 7 were used for manufacturing the steel stamping dies in Computer Numer-

ical Control (CNC) milling machine. All die-punch pairs and the resulting stamped parts are shown in Figure 13. [AQ7]

Figure 13. Steel CNC milled die-punch pairs and prototype's stamped parts.

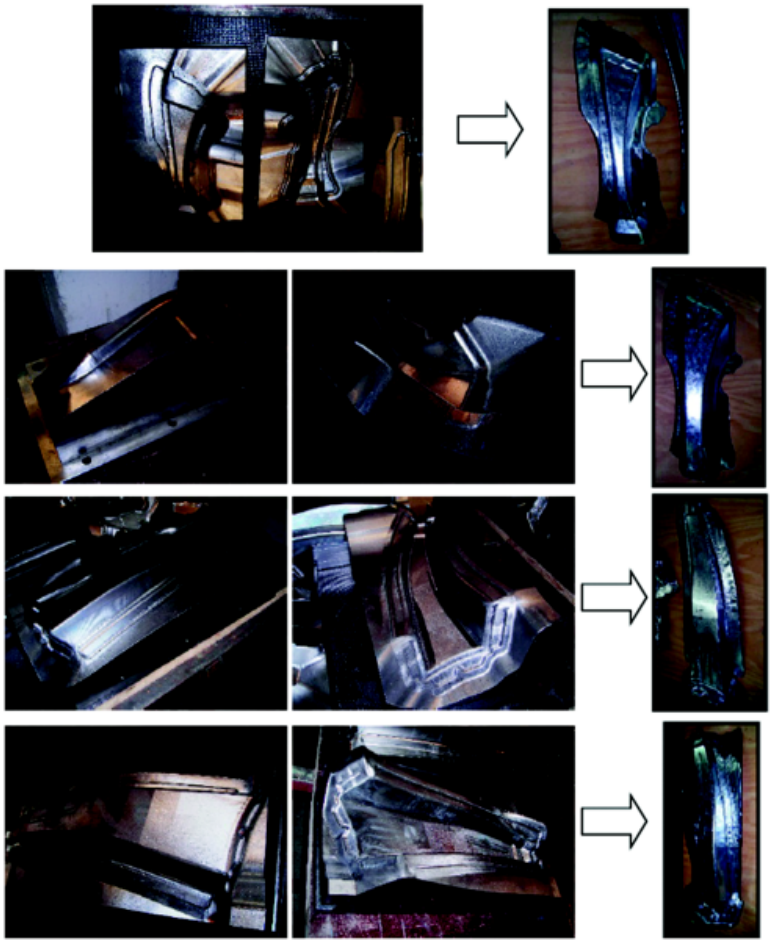

The four steel skins were stamped using cold-formable low-carbon steel EN10346:2015 [13] DX51D in 0.5-mm-thick sheets; then, the sandwich structures were created filling each inner-outer pair with a standard low density epoxy foam Sicomin PB170 DM02 [14]. While being in viscous state, this bi-component resin was introduced by gravity at each foam cavity, and later on, it expanded and turned into solid foam inside the sandwich due to the polymerization reaction (in this case, 48 hours at ambient temperature plus 24 hours at 40°C). Finally, and after the curing process, the bonding between upper and lower pillar was achieved applying a bi-component polyurethane adhesive SikaForce-7752 L90 [15] between the surfaces in contact at the connection region. Table 16 shows the mechanical properties in these materials comprising the prototype. Figure 14 shows images of the filling and the bonding process during the prototypes' manufacture. The total mass of the C-pillar sandwich prototype was 1.334 kg, value slightly higher than the original design (1.254 kg).

Table 16. Mechanical properties of the prototype's materials.

	Density (kg/m^3)	Elastic modulus (MPa)	Poisson's ratio	Tensile strength (MPa)	Elongation at break (/1)
Steel EN10346 DX51D	7800	210,000	0.3	270[a]	0.18[a]

	Density (kg/m^3)	Elastic modulus (MPa)	Poisson's ratio	Tensile strength (MPa)	Elongation at break (/1)
Sicomin PB170 DM02	170	128[b]	0.3	1.7[b]	0.02[b]
SikaForce-7752 L90	1520[c]	–	0.3	10	0.2

[a]Values obtained from the steel supplier's certification.

[b]Flexural properties.

[c]According to components proportion.

Figure 14. Left: filling process in lower pillars and right: upper and lower pillars assembled by pressure during the adhesive curing.

Finally, two parts adjacent to C-pillar were included into test specimens: the left "assembly to roof" part at the top and a portion of the structural part covering the rear left wheel at the bottom. Both parts were fixed by means of rivets instead of the welding points. Since the objective of these tests was more to check the stiffness performance of the prototypes than to obtain the stress values reached, this assembly procedure was considered adequate.

The final specimen was mounted and screwed on a resin and wood support specifically manufactured for fixing the prototype to the test bench. Figure 15 shows the test configuration: the displacement was applied with an angle of 30° in relation to the transversal axis of the vehicle by means of a screwed fastener, transforming the rotation of its inner screw into translation. A load cell was placed between the fastener and the specimen for measuring the resulting force. Finally, the fastener's end was hooked to a steel post, clamped to the test bench, and designed with an adequate height for achieving a 30° angle for the force direction.

Figure 15. Left: test configuration.

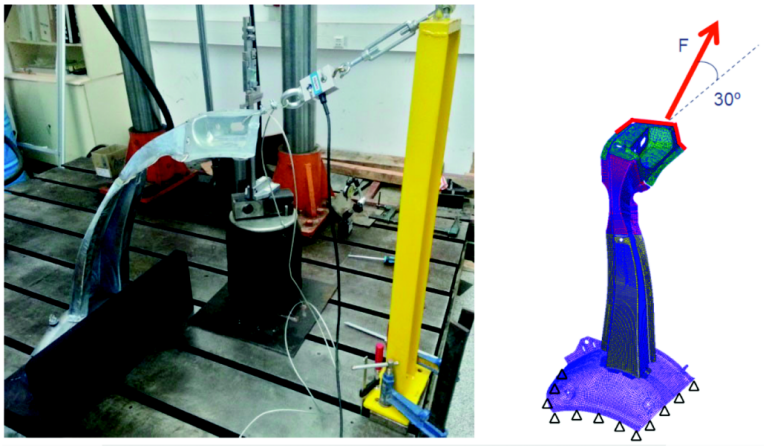

Two uniaxial extensiometric gauges were bonded to one of the specimens in order to measure the micro-strain values reached at two points located on the outer surfaces of the upper and lower C-pillar. Figure 16 shows the position of these gauges on the prototype.

Figure 16. Extensiometric gauges' position at upper and lower C-pillars (mm).

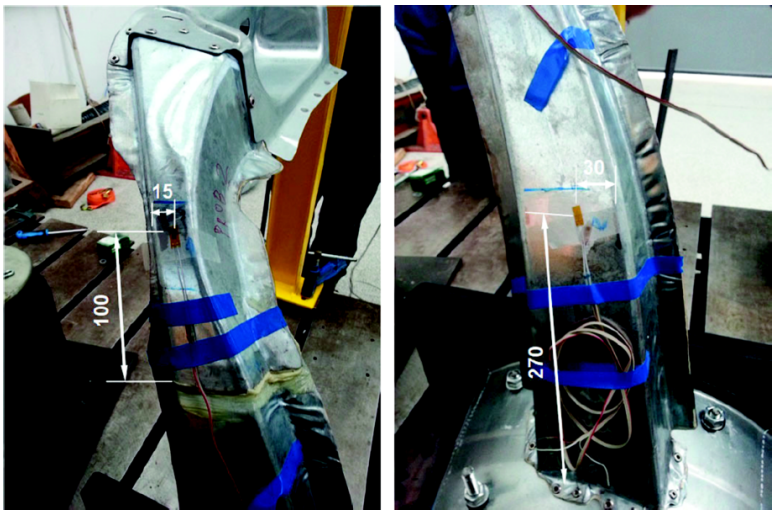

Three samples were tested at Zaragoza University facilities. The force–displacement graphs obtained for the three specimens are gathered in Figure 17, and the micro-strain values obtained from the second specimen tested are shown in Figure 18. Table 17 details the strain values registered at 100, 200, 300, and 350 scans in test 2 as well as the force values measured with the load cell for each of these scanning numbers.

Figure 17. Force–vertical displacement results for the three specimens tested and the numerical FE model.

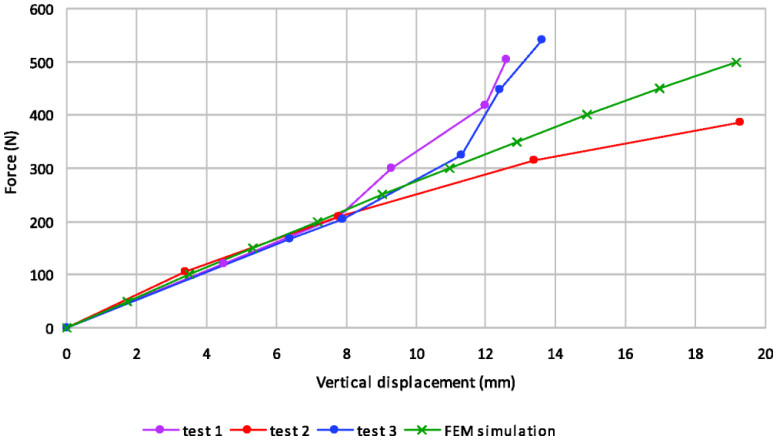

Figure 18. Strain results obtained at the extensiometric gauges in the second specimen tested (gauge 1 at upper C-pillar and gauge 2 at lower C-pillar).

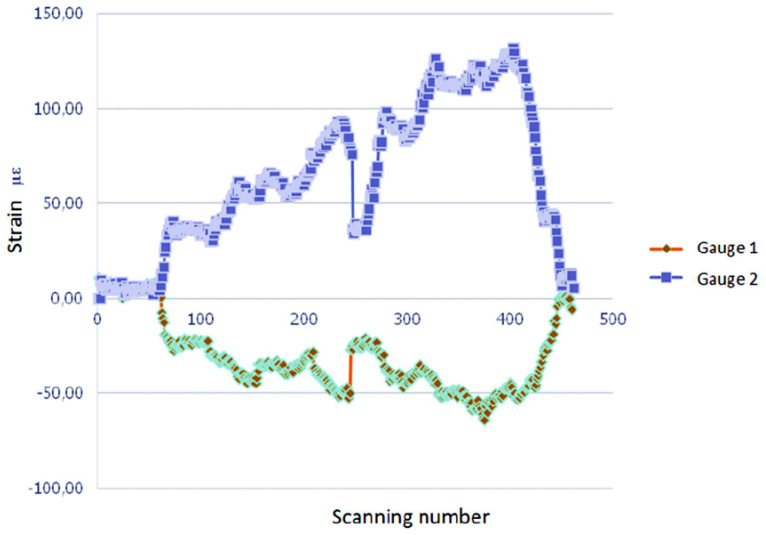

Table 17. Strain values at gauges 1 and 2 at different force values in test 2.

Scanning number	Force (N)	Strain gauge 1 (με)	Strain gauge 2 (με)
100	106	–22.77	35.76
200	208	–31.54	64.90
300	314	–44.44	84.99
350	386	–48.03	112.78

From Figure 17, it can be observed that the three specimens' vertical displacements performed quite similarly until reaching a force value of 200 N. From that point on, an increase in force value corresponded to different vertical displacements at each specimen tested: while specimens 1 and 3 showed maximum displacements ranging from 12 to 14 mm for 500 N, specimen 2 performed less rigidly, reaching a maximum displacement of 19.3 mm for 386 N. The numerical results obtained with the FE model analyzed are also included in Figure 17. Ten static analyses were run applying the same boundary conditions and different force values: 50, 100, 150, 200, 250, 300, 350, 400, 450, and 500 N. As can be observed, numerical displacement values were very similar to the test values until reaching approximately 200 N. However, at higher force levels, vertical displacement values were located halfway between test 1 and test 2 values. Figure 19 shows the vertical displacements distribution (z axis in the model) obtained in the numerical model for two of the load cases analyzed: 200 N and 500 N.

Figure 19. Vertical displacement values obtained numerically for force values 200 N and 500 N.

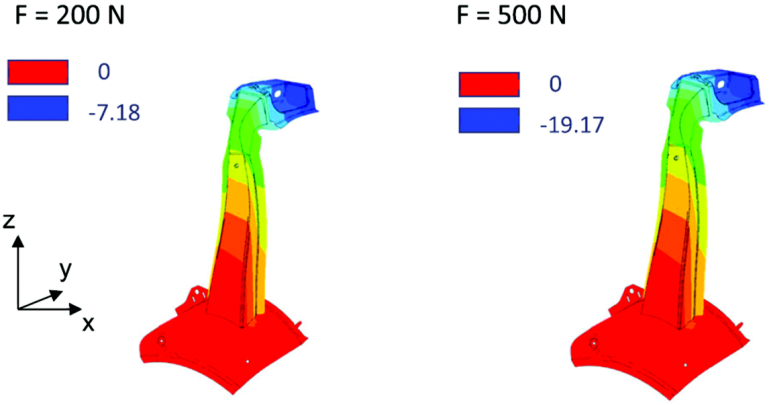

Finally, the strain values measured with the extensiometric gauges in test 2 (Figure 16) were compared with the strain values obtained at the same locations in the numerical model analyzed. For instance, while the experimental strain obtained at gauge 1 (upper C-pillar) was –22.77 με for a force of 106 N, the numerical strain at that position was –39.9 με for the load case with 100 N. As for the lower C-pillar, while the experimental strain obtained at gauge 2 was +35.76 με for a force of 106 N, the numerical strain at that position was +22 με for the load case with 100 N. Although the obtained numerical values were not equal to the experimental ones, they were quite close and achieved to represent the strain progression during the test quite properly.

As a result of this experimental–numerical validation, it was considered that the numerical model was able to reproduce C-pillar's rigidity response appropriately, mainly at force values below 200 N. At higher force values, the tested specimens performed differently, probably due to geometrical and material irregularities generated during their manufacture process.

Conclusions

Results of a research project carried out in close collaboration between the University of Zaragoza and the Spanish car manufacturer SEAT are shown in the present article.

From a C-pillar made nowadays of stamped steel, mechanical behavior of six new different C-pillar configurations was studied. The new C-pillars were constructed as a sandwich structure with steel skins and 10 mm of rigid polymer foam core or 3 mm polymer sandwich core. Some of studied configurations included some cross-shaped foldings embossed on inner skins for the 3 mm and 10 mm thickness C-pillars. Additionally, it was studied a final configuration incorporating an optimal connection region between upper and lower pillars, including flanges to connect inner and outer skins between each other in order to avoid hinge effect at that area. FEM models of all the analyzed configurations of C-pillar were developed.

Two load cases were applied for assessing the torsional stiffness of C-pillars. On one hand, first load case consists of displacement results obtained at several reference points when an overall torsional load is applied to the complete vehicle including the current C-pillar. On the other hand, second load case consists of imposing a torsional angle of 1° in the upper border of the C-pillar, while the lower border is clamped.

Specific stiffness (N/mm kg) of each analyzed C-pillar was obtained numerically under both load cases.

Comparing the different values obtained for the different models in terms of reaction force and moment, mass, and specific stiffness, it was found that C-pillar design number 3 (sandwich structures with 10-mm rigid polymer foam core and 0.4 mm steel skins) had the best performance in terms of torsional stiffness. A mass reduction of 0.243 kg (18.9%) and a stiffness increase of 292 N/mm·kg (38.1%) were achieved. However, it has been stated that the inclusion of cross-shaped foldings embossed at inner skins of sandwich structures did not contribute positively neither for C-pillar with 3-mm thermoplastic core nor for the one with 10-mm polymer core.

It was concluded that a thickness increase for lower pillar was more effective than a thickness increase for upper pillar. Additionally, when applying sandwich structure on upper and lower C-pillar, the joint region connecting both pillars had to be redesigned including an overlap between them in order to improve the momentum of inertia in the joint zone. Otherwise, this region resulted as a weak point to flexural loads once sandwich structures were included, showing non-desirable hinge effects in it.

Specifically, sandwich structures with 0.4 mm steel skins and 10 mm rigid foam core, including the new connection region and welding flanges for both inner and outer skins, were the best design option. Not only did they have the lowest mass values, but they also achieved quite higher reaction forces and moments. This mechanical performance was verified in a more complete structural model including two adjacent parts, obtaining a 64% increase in specific stiffness for the first load case corresponding to vehicular displacements and a 363% increase in the second load case related to specific torsional stiffness for the rotational 1° angle.

Three sandwich C-pillar prototypes were manufactured by means of low cost molds, in order to carry out tests with them, applying a load similar to the existing load in the first displacement load case. Global displacement and strain values were measured by using dial and extensiometric gauges in testing. These values were compared with the corresponding ones obtained at the same locations in the numerical model analyzed. The comparison was carried out for different instants throughout the loading process. Taking into account the high experimental–numerical correla-

tion, it was considered that the numerical model was able to reproduce stiffness response of C-pillar properly, mainly at force values below 200 N.

Declaration of Conflicting Interests

The author(s) declared no potential conflicts of interest with respect to the research, authorship, and/or publication of this article.

Funding

The author(s) disclosed receipt of the following financial support for the research, authorship, and/or publication of this article: The authors would like to thank SEAT company for funding this R+D project.

ORCID iDs

David Valladares https://orcid.org/0000-0002-6046-4558

Luis Castejon https://orcid.org/0000-0002-9007-1560

David R Angulo https://orcid.org/0000-0001-8451-660X

References

1. Mazzon E, Habas-Ulloa A and Habas JP. Lightweight rigid foams from highly reactive epoxy resins derived from vegetable oil for automotive applications. Eur Polym J 2015; 68: 546–557.

2. Fremgen C, Mkrtchyan L, Huber U, et al. Modeling and testing of energy absorbing lightweight materials and structures for automotive applications. Sci Technol Adv Mater 2005; 6: 883–888.

3. Patel JM and Modi BA. Stiffness and thermal analysis of doubly curve sandwich panel for an automobile application (Chemical, civil and mechanical engineering tracks of 3rd Nirma University international conference on engineering (NUICONE2012)). Procedia Eng 2013; 51: 655–664.[AQ8]

4. Cameron CJ, Wennhage P, Goransson P, et al. Structural-acoustic design of a multi-functional sandwich panel in an automotive context. J Sandw Struct Mater 2010; 12: 684–708.

5. Aly MF, Hamza KT and Farag MM. A materials selection procedure for sandwiched beams via parametric optimization with applications in automotive industry. Mater Des 2014; 56: 219–226.

6. Vogel J, Keller J, Sviridov A, et al. Characterisation of strength behaviour of aluminium foam sandwiches under static load. Strain 2011; 47(Supplement 1): E234–E242.

7. Mkrtchyan L, Maier M and Huber U. Structural polyurethane foam: testing and modelling for automotive applications. Int J Crashworthiness 2008; 13: 523–532.

8. Dupuis R, Duboeuf O, Kirtz B, et al. Characterization of vibrational mechanical properties of polyurethane foam. Dyn Behav Mater 2016; 1: 123–128.

9. Pasha HG, Allemang RJ, Brown DL, et al. Static torsional stiffness from dynamic measurements using impedance modeling technique. Chapter. Dynamics of coupled structures. In: *Part of the series conference proceedings of the society for experimental mechanics series*, 2014, Volume 1, pp.307–316.[AQ9]

10. Porsche Engineering Services, Inc. *Ultra-light steel auto body (ULSAB). Phase 2 findings*. Report, March 1998, Version 1.0.2.[AQ10]

11. Caprino G and Teti R. Sandwich structures handbook. Italy: Edizioni Il Prato, 1989.

12. AENOR. Standard UNE-EN10268:2006+A1:2013. Cold rolled steel flat products with high yield strength for cold forming. Technical delivery conditions.

13. AENOR. Standard UNE-EN10346:2015. Continuously hot-dip coated steel flat products for cold forming - Technical delivery conditions.

14. Sicomin Epoxy Systems. Technical datasheet. PB foaming epoxy. Version 24/01/2014. PB 170, PB 250, PB 400, PB 600 cellular epoxy foam production systems, http://www.sicomin.com/datasheets/product-pdf188.pdf (accessed 3 November 2018).

15. SIKA, S.A.U. *Hoja de datos de producto. Versión 03/2007. SikaForce - 7752 L90. Adhesivo estructural tixotrópico*. Alcobendas: Author, pp.125–126.[AQ11]